Dissociation energies of gold clusters Au_N^+, $N=7-27$

K. Hansen
Department of Physics, Göteborg University, SE-412 96 Göteborg, Sweden

A. Herlert* and L. Schweikhard
Institut für Physik, Ernst-Moritz-Arndt-Universität, D-17487 Greifswald, Germany

M. Vogel†
Institut für Physik, Johannes-Gutenberg-Universität, D-55099 Mainz, Germany
(Received 16 February 2006; published 13 June 2006)

Unimolecular decay rates and monomer-dimer branching ratios of gold clusters Au_N^+ ($N=7-27$) have been measured as a function of excitation energy in photodissociation experiments on size-selected clusters stored in a Penning trap. Part of the data set has previously been used to extract model-free values of dissociation energies [Vogel *et al.*, Phys. Rev. Lett. **87**, 013401 (2001)]. Other parts of the data set do not allow this analysis. We use these data to extract tentative dissociation energies, based on the systematics of deviations between an Arrhenius analysis and the model-free values. The observed systematics also allows an estimate of the true frequency factor which often is much higher than the Arrhenius value but in good agreement with the expected detailed balance value. The data are also reanalyzed including radiative cooling which may explain part of the discrepancy between model-free and Arrhenius dissociation-energy values.

DOI: 10.1103/PhysRevA.73.063202 PACS number(s): 36.40.Qv, 36.40.Wa

I. INTRODUCTION

Gold clusters in general and their stability in particular have been investigated for a considerable period of time [1–19]. One reason for this extensive interest is the potential application of gold surfaces and clusters in, e.g., catalysis [13]. At the same time, gold remains a challenge for theorists because relativistic effects play an important role for the electronic and geometric structures [20–33]. As with other monovalent metal clusters, gold clusters show shell structure and odd-even effects in the binding energies [1,7]. These are observed in measurements of ionization potentials [8] and photoelectron spectroscopy [6,9], where the electronic structure is probed directly, as well as in abundance spectra of hot, evaporating clusters [1,7]. The abundance spectra reflect the total binding energy of clusters, B_N, with respect to N free atoms. This, in turn, is determined by an interplay between geometric [3,4,10,12,23,24,27–29] and electronic structure [1,5,27,29,34] of the particle. Experimental values of the binding energy would therefore provide a stringent test of theoretical structure calculations. Unfortunately, the total binding energy is difficult to determine experimentally for all but the smallest clusters. Alternatively, one may measure the differential binding energy, $D_N=B_N-B_{N-1}$. In the absence of an activation energy for the attachment of an atom to a cluster of size $N-1$, this difference in ground state energies is also the energy barrier (activation energy) for the evaporation of an atom from the cluster of size N. The dissociation energy D_N can be probed by use of evaporative processes, because the rate of these depends strongly on the value of the dissociation energy. One method is to use metastable fragmentation probabilities [35,36]. Another, related method, is to use abundance variations in ensembles with broad mass distributions to extract dissociation energies [37–39]. Unfortunately, only relative variations can be obtained with these methods unless a calibration to absolute energies can be found.

Alternatively, if energy-resolved decay rate constants, $k_N(E)$, are available, one may extract the dissociation energies by simple inversion of the theoretical expression for $k_N(E)$. However, the conversion from measured rate constants to activation energies is not completely straightforward. Even disregarding the ambiguity presented by the considerable number of different expressions for $k_N(E)$ on the one hand, and the potential experimental problems with, e.g., preparing samples with a well-defined excitation energy on the other, one may still encounter systematic uncertainties in the modeling.

One of those uncertainties is the possibility of a competing decay channel. For size-selected cationic metal clusters most problems of this kind are posed by radiative cooling [40–45] which is not easily observed directly. Another uncertainty is the level density of the clusters involved in a decay process. Any realistic expression for the evaporative rate constant requires knowledge of the level densities of the precursor and the product. Whereas these functions are computable for small molecules for which spectroscopy has provided good values for the vibrational frequencies, this is rarely the case for clusters. For example, clusters may have a phase transition akin to bulk melting [46,47], with parameters which are size dependent and can be different for precursor and product. This imparts some systematic uncertainty in the dissociation energies extracted from rate constants with the use of standard level densities.

*Present address: Physics Department, CERN, 1211 Geneva 23, Switzerland.
†Present address: GSI, Planckstrasse 1, 64291 Darmstadt, Germany.

It is therefore highly desirable to have methods available which are independent of the level density or the caloric curve. This is accomplished with a recently developed method to measure the dissociation energies [14–19,48]: It is based on a comparison of sequential and simple decays that lead to the same product. This "model-free" method has been used to determine the dissociation energies of gold clusters Au_N^+ ($N=8,14-25$) with an accuracy better than 5%.

The availability of precise dissociation energies allows tests of the assumptions that are used to calculate rate constants for the specific systems. With an expression for the rate constant as a function of the excitation energy and the dissociation energy, the dissociation energy can be found by solving this equation with the values measured experimentally for a given excitation energy. This should yield dissociation energies independent of the excitation energies. However, the application of both detailed-balance theory [49–51] and RRKM theory [52–54] to the measured rate constants give fitted values of the dissociation energies that depend on the excitation energy [14], less strongly for the detailed-balance rate constant, but still with a statistically significant amount. In general, a variation of the activation energy in rate expressions is not impossible, e.g., when electronic excitations are taken into account [55–59], but the magnitude of the variation observed here is much larger than expected from this effect. As another indication of nontrivial behavior, Arrhenius-type plots result in frequency factors which are up to eight orders of magnitude smaller than the Debye frequency of the bulk, and more than ten orders of magnitude smaller than the expected frequency factor in any approximate Arrhenius expression, like the detailed-balance rate constant used in the following. Similarly, the fitted values of the dissociation energies are up to a factor 4 too low. The Arrhenius plots rely on a conversion of the excitation energy to an effective temperature, i.e., for this conversion a caloric curve must be entered.

These problems indicate that one or more of the assumptions, the shape of the caloric curve and/or the absence of competing channels, is incorrect. In the following, an extended set of time-resolved photodissociation measurements on gold clusters Au_N^+ ($N=7-27$) will be presented, and the possible explanations for the failure of the theoretical expressions will be examined. In addition, the dissociation energy for cluster sizes for which the model-free values have not been measured, but for which decay-rate constants are available, will be calculated based on the systematics of the model-free values and on a parametrization of the error in the Arrhenius plots of the observed rate constants.

II. EXPERIMENTAL SETUP AND PROCEDURES

The cluster ions are produced in a laser vaporization source [60] and transferred to a Penning trap where they are stored and size-selected by resonant ejection of all other ions. The size-selected ensemble is centered radially and thermalized to the trap temperature by use of argon gas pulses [61]. The clusters are photoexcited with a pulsed Nd:YAG-pumped dye laser (frequency-doubled when needed), with a pulse length around 10 ns. The laser can be tuned to photon energies from 2 to 6 eV. After a variable delay period between 10 μs and 60 ms the remaining precursor and fragment abundances are analyzed in a time-of-flight (TOF) mass spectrometer with single-ion counting in a Daly-type detector. More details on the experimental setup and procedure can be found in Refs. [62–65]. As an example, Fig. 1 shows TOF spectra before and after photoexcitation of Au_7^+ clusters. By variation of the storage period between photoexcitation and ejection it is possible to monitor the delayed dissociation process time-resolved.

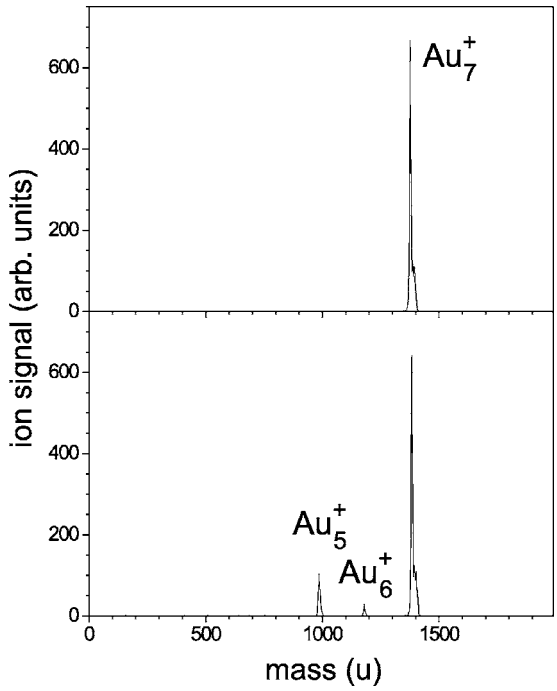

FIG. 1. Top: Mass-selected ensemble of Au_7^+ cluster ions before photoexcitation. Bottom: Product spectrum 60 ms upon laser excitation with a photon energy of $E_\gamma=3.49$ eV at a pulse energy of 30 μJ.

For monovalent metal clusters such as gold clusters two decay channels are observed, depending on the cluster size and excitation energy: neutral monomer and neutral dimer evaporation [66–70]. In some cases there is an energy-dependent competition between the two channels [71,72]. For $N=3$ and $N=5$ gold-cluster cations, dimer evaporation is the only observed decay pathway, while for all even-size cluster cations and for $N>15$ only monomer evaporation has been observed [71]. For odd-size cluster cations in the intermediate region from $N=7$ to $N=15$ neutral dimer evaporation competes with neutral monomer evaporation [66–69,71,72]. As an example, the case of Au_{13}^+ is shown in Fig. 2, where the relative intensities of initial and product clusters are plotted as a function of the delay time between photoexcitation of Au_{13}^+ clusters and ejection for mass analysis. Both monomer decay $Au_{13}^+ \rightarrow Au_{12}^+ + Au$ and dimer decay $Au_{13}^+ \rightarrow Au_{11}^+ + Au_2$ are observed.

Figure 3 shows an example for a sequential decay, the dissociation of Au_{25}^+. Photoexciation leads to a decay to

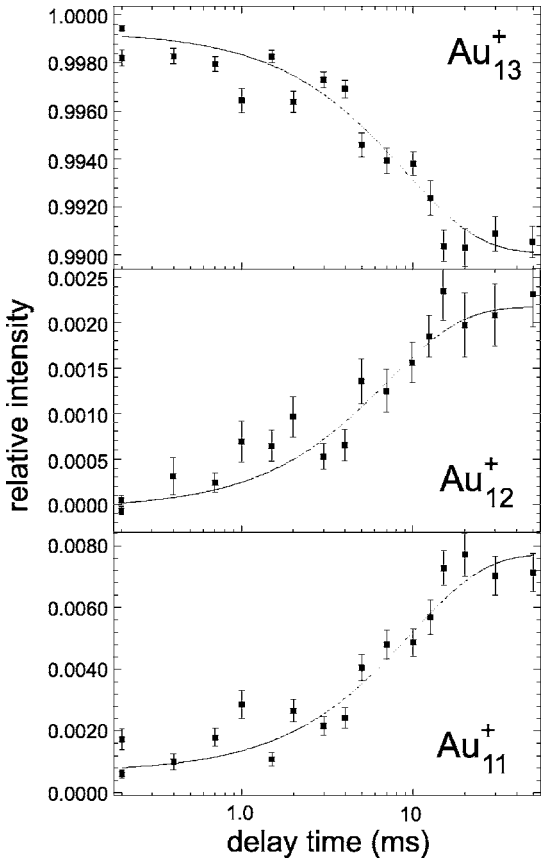

FIG. 2. Initial and product cluster intensities as a function of delay time between laser excitation and detection for mass-selected Au_{13}^+ cluster ions irradiated with a laser pulse of 50 μJ at a photon energy of 4.40 eV. The lines are exponential fits to the data (note the logarithmic abscissa).

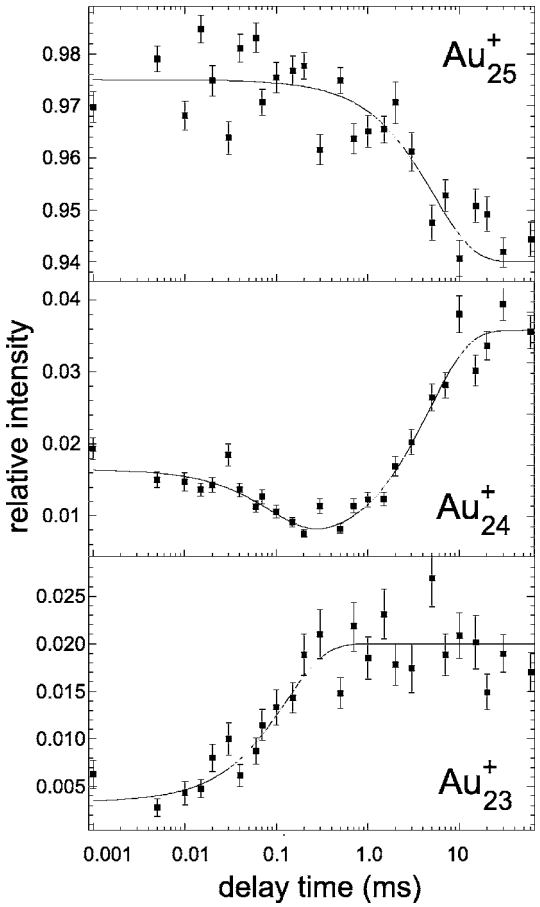

FIG. 3. Initial and product cluster intensities as a function of delay time between laser irradiation and detection for mass-selected Au_{25}^+ cluster ions irradiated with a laser pulse of 120 μJ at a photon energy of 3.99 eV. The lines are fits to the data with a single exponential decay or two sequential decay-growth curves as described in the text.

Au_{24}^+ and then further to Au_{23}^+. Note that in contrast to a competition of decay pathways the decay and appearance rates of precursors and products in general have different values. In addition, the intermediate fragment Au_{24}^+ shows a finite abundance at the shortest measured delay time due to the fast first step of the sequential decay on time scales outside the experimental time window, i.e., shorter than approximately 10 μs. In this particular case both the decay from Au_{25}^+ to Au_{24}^+ (absorption of two photons, see Table I) and the further decay from Au_{24}^+ to Au_{23}^+ (absorption of three photons, see Table II) is observed. For a detailed discussion of the general characteristics of a sequential decay in the Penning trap, see, e.g., Ref. [73].

For one-step decays, the measurement also yields the relative pathway intensities of product clusters Au_{N-1}^+ and Au_{N-2}^+, f_1 and f_2, respectively, with $f_1+f_2=1$, as listed in Table I. The branching ratios are independent of delay time [72] and thus the values listed in the table are the average values for the investigated delay times. In most cases the large number of counts included in the averaging gives a low statistical uncertainty which will be ignored in the following. For a few cases, however, indicated by "-," only the decay rate constant is determined from the precursor yields.

III. EXPERIMENTAL RESULTS

Table I gives the measured decay rates of Au_N^+ ($N=7-27$) as a function of the photoexcitation energy E_γ. The total excitation energy E_{tot} is given by the sum of the photoexcitation energy E_γ and the initial thermal energy E_{th} of the cluster before laser irradiation. For the present room-temperature experiment the latter is set to $E_{th}=N_{eff}\times 0.063$ eV, based on an extrapolation from the bulk heat capacity [14]. $N_{eff}=N-2$ is the effective number of atoms in the cluster that contribute to the heat capacity. The use of N_{eff} is warranted if the heat capacity is carried by the motion of the nuclei. Since the heat capacity of the valence electrons is very small at room temperature, this should be a good approximation.

Table II gives the rate constants of the final decay step in two-step sequential decays of the type $Au_N^+ \rightarrow Au_{N-1}^+ \rightarrow Au_{N-2}^+$, i.e., the appearance rates of the Au_{N-2}^+ signals. As described earlier, the first decay occurs very fast as compared to the time scale of the last decay which can be observed time-resolved. Therefore, the first decay has no influence on the determination of the dissociation rate in the last decay of the sequence [17].

TABLE I. Experimental values for the decay rate k of the initial cluster Au_N^+ and the relative fragment yields of direct fragments Au_{N-1}^+ (f_1) and Au_{N-2}^+ (f_2) as a function of excitation energy $E_{tot}=E_\gamma+E_{th}$. In this and all other tables, the number in the parentheses is the 1-σ uncertainty in units of the last digit given.

N	E_γ (eV)	E_{tot} (eV)	k (10^3 s^{-1})	f_1	f_2
	3.31	3.62	2.6(5)	0.03	0.97
7	3.40	3.71	5.3(11)	⋯	⋯
	3.50	3.81	9.1(9)	0.04	0.96
	2.56	2.94	1.9(7)	1	0
	2.59	2.97	2.8(8)	1	0
8	2.64	3.02	4.9(8)	1	0
	2.70	3.08	8.6(16)	1	0
	2.76	3.14	13(4)	1	0
	2.82	3.20	16(3)	1	0
	3.65	4.09	0.07(1)	0.16	0.84
	3.81	4.25	0.19(3)	0.17	0.83
9	4.00	4.44	2.7(5)	0.20	0.80
	4.21	4.65	10(4)	0.25	0.75
	4.40	4.84	59(14)	0.30	0.70
	2.53	3.03	0.18(7)	1	0
	2.59	3.09	0.33(6)	1	0
	2.64	3.14	0.55(14)	1	0
10	2.70	3.20	0.90(17)	1	0
	2.76	3.26	2.3(3)	1	0
	2.90	3.40	9.5(14)	1	0
	2.95	3.45	14.3(16)	1	0
	3.60	4.17	0.15(5)	0.04	0.96
	3.81	4.38	0.41(6)	0.06	0.94
11	4.00	4.57	1.5(3)	0.07	0.93
	4.10	4.67	3.7(6)	⋯	⋯
	4.21	4.78	18(2)	⋯	⋯
	4.40	4.97	24(12)	0.07	0.93
	3.60	4.23	2.5(13)	1	0
12	3.81	4.44	5.5(10)	1	0
	4.00	4.63	12(2)	1	0
	4.10	4.73	14(3)	1	0
	4.40	5.09	0.13(5)	0.19	0.81
	4.51	5.20	0.14(2)	0.20	0.80
13	4.70	5.39	0.19(2)	0.24	0.76
	5.00	5.69	0.52(8)	0.29	0.71
	5.30	5.99	8.8(18)	0.39	0.61
	3.65	4.41	0.11(1)	1	0
	3.81	4.57	0.13(3)	1	0
	3.99	4.75	0.19(2)	1	0
14	4.21	4.97	0.35(4)	1	0
	4.40	5.16	1.03(13)	1	0
	4.51	5.27	2.0(3)	1	0
	4.70	5.46	3.0(5)	1	0

TABLE I. (*Continued.*)

N	E_γ (eV)	E_{tot} (eV)	k (10^3 s^{-1})	f_1	f_2
	5.30	6.12	0.23(2)	0.67	0.33
15	5.64	6.46	0.76(5)	0.77	0.23
	6.02	6.84	5.7(8)	0.80	0.20
	3.99	4.87	0.06(2)	1	0
	4.51	5.39	0.12(2)	1	0
16	4.70	5.58	0.17(2)	1	0
	5.00	5.88	0.30(3)	1	0
	5.30	6.18	1.4(2)	1	0
	5.64	6.52	6.6(4)	1	0
	3.99	4.93	0.04(3)	1	0
	4.51	5.45	0.05(2)	1	0
	5.30	6.24	0.06(1)	1	0
17	5.64	6.58	0.20(1)	1	0
	6.02	6.96	0.68(5)	1	0
	2·3.49	7.93	6.9(9)	1	0
	3.99	5.00	0.04(2)	1	0
	5.30	6.31	0.15(2)	1	0
18	5.64	6.65	0.24(2)	1	0
	6.02	7.03	0.32(5)	1	0
	2·3.99	8.99	1.6(4)	1	0
	6.02	7.09	0.04(1)	1	0
19	2·3.49	8.06	1.4(2)	1	0
	2·3.99	9.05	27(7)	1	0
	5.30	6.43	0.09(1)	1	0
	5.64	6.77	0.18(2)	1	0
20	6.02	7.15	0.26(3)	1	0
	2·3.49	8.12	1.7(3)	1	0
	2·3.99	9.11	3.5(7)	1	0
	2·3.49	8.19	0.12(1)	1	0
21	2·4.10	9.40	2.7(5)	1	0
	2·4.21	9.62	5.7(9)	1	0
	6.02	7.28	0.11(2)	1	0
22	2·3.49	8.25	0.79(8)	1	0
	2·4.10	9.46	15(3)	1	0
23	2·4.10	9.52	1.1(1)	1	0
	2·4.21	9.74	2.7(5)	1	0
	2·3.49	8.37	0.09(2)	1	0
24	2·4.10	9.58	0.75(14)	1	0
	2·4.21	9.80	1.43(17)	1	0
	2·4.40	10.18	2.3(3)	1	0
	2·3.99	9.43	0.19(3)	1	0
	2·4.10	9.65	0.21(4)	1	0
	2·4.21	9.87	0.20(5)	1	0
25	2·4.40	10.25	0.40(8)	1	0

TABLE I. (*Continued.*)

N	E_γ (eV)	E_{tot} (eV)	k (10^3 s^{-1})	f_1	f_2
	2·5.00	11.45	1.9(4)	1	0
	3·3.49	11.92	22(3)	1	0
26	2·4.21	9.93	0.28(14)	1	0
27	2·4.51	10.59	0.35(13)	1	0

Table III gives the rate constants of the final decay in three-step sequential decays of the kind $Au_N^+ \rightarrow Au_{N-1}^+ \rightarrow Au_{N-2}^+ \rightarrow Au_{N-3}^+$. Again, the first two decays do not have any effect on the determination of the dissociation rate in the last decay of the sequence.

TABLE II. Experimental values for the appearance rate constants of fragments Au_{N-2}^+ in two-step sequential decays as a function of excitation energy $E_{\mathrm{tot}}=E_\gamma+E_{\mathrm{th}}$.

N	E_γ (eV)	E_{tot} (eV)	k (10^3 s^{-1})
14	2·3.99	8.74	0.24(5)
	2·3.49	7.81	0.11(2)
15	2·3.99	8.80	0.79(13)
	2·4.18	9.18	3.4(13)
	2·4.30	9.42	42(16)
	2·3.99	8.86	0.06(1)
	2·4.21	9.30	0.7(2)
16	2·4.30	9.48	1.78(18)
	2·4.40	9.68	5(2)
	2·4.51	9.90	5.2(12)
	2·3.99	8.92	0.04(1)
17	2·4.21	9.36	0.26(7)
	2·4.30	9.54	0.65(15)
	2·4.51	9.96	4.4(7)
	2·3.99	8.99	0.04(3)
18	2·4.51	10.03	0.24(4)
	2·5.00	11.01	1.9(5)
19	2·5.00	11.07	0.36(6)
20	2·5.00	11.13	0.20(4)
	3·3.49	11.61	0.99(8)
21	2·5.00	11.20	0.36(6)
	2·5.00	11.26	0.10(1)
22	3·3.49	11.74	0.70(7)
	3·3.99	13.23	3.0(5)
23	2·5.00	11.32	0.13(1)
	3·3.49	11.80	0.70(10)
24	3·3.49	11.86	0.07(2)
25	3·3.99	13.41	9(2)

The data set in the tables above-mentioned were used to determine dissociation energies by the method mentioned in Sec. I and described in detail in Refs. [14–19]. One version of this method uses the monitoring of the decay rate constants as a function of excitation energy. Sequential decays of the type

$$A \rightarrow B \rightarrow C \tag{1}$$

(see Table II) are compared to the decay involving only B and C,

$$B \rightarrow C \tag{2}$$

(see Table I) such that the reaction $B \rightarrow C$ takes place at the same rate constant k. Effectively, the process in Eq. (2) acts as a calorimeter. When the two excitation energies in Eqs. (1) and (2) are tuned to give identical values of k, the dissociation energy, D_{mf}, is given by $D_{\mathrm{mf}}=\Delta E_\gamma - K + \Delta E_{\mathrm{th}}$, where ΔE_γ is the difference in photon excitation energy of the two clusters, K is the kinetic energy release, and ΔE_{th} is the difference in initial thermal energy of A and B. This method has been used to determine the dissociation energies of gold clusters Au_N^+ ($N=8, 14-25$) with an accuracy of a few % (see Table IV). The resulting uncertainty is small because the rate constants depend very strongly on the excitation energy.

TABLE III. Experimental values for the appearance rate constants of fragments Au_{N-3}^+ in three-step sequential decays as a function of excitation energy $E_{\mathrm{tot}}=E_\gamma+E_{\mathrm{th}}$.

N	E_γ (eV)	E_{tot} (eV)	k (10^3 s^{-1})
17	3·3.99	12.91	0.10(3)
18	3·3.99	12.97	0.22(4)
	3·4.30	13.91	11(2)
19	3·4.30	13.97	0.10(2)
	3·4.51	14.59	0.67(7)
	3·4.10	13.43	0.06(2)
20	3·4.30	14.03	0.14(4)
	3·4.51	14.66	0.29(5)
21	3·4.30	14.09	0.03(1)

TABLE IV. Measured energy differences ΔE_γ, calculated kinetic energy releases $K(N)$ and model-free dissociation energies $D_{\mathrm{mf}}(N) = \Delta E_\gamma - K(N) + \Delta E_{\mathrm{th}}$ for clusters Au_N^+ [$N=8,14-25$ (monomer evaporation) and $N=9,11,13,15$ (dimer evaporation)]. For dimer evaporation the term $K(N)$ also includes the energy loss in the rotational and vibrational modes of the emitted dimer. The abbreviations in the "Method" column refer to the calorimeter process: R=rate constants, B=monomer-dimer branching ratio, and the length of the decay chain: S=single sequential decay, M=multisequential decay.

N	ΔE_γ (eV)	$K(N)$ (eV)	$D_{\mathrm{mf}}(N)$ (eV)	Method	Reference
			Monomer dissociation		
8	3.05(6)	0.46(5)	2.65(8)[a]	BS	[62]
14	3.25(8)	0.13(3)	3.18(9)[a]	RS	[14]
	3.31(5)	0.13(3)	3.24(6)[a]	BS	[15]
15	3.65(10)	0.19(3)	3.52(10)	RS	[14]
16	3.12(9)	0.18(3)	3.00(10)[a]	RS	[14]
	3.15(7)	0.18(3)	3.03(8)[a]	BS	[15]
17	3.47(6)	0.16(2)	3.37(6)[b]	RS	[14]
	3.70(7)	0.38(4)	3.38(8)	RM	[17]
18	3.41(6)	0.17(2)	3.30(6)	RS	[14]
	3.54(8)	0.32(3)	3.28(9)	RM	[17]
19	3.95(7)	0.22(2)	3.79(7)	RS	[14]
	4.10(8)	0.33(3)	3.83(9)	RM	[17]
20	3.62(8)	0.19(2)	3.49(8)	RS	[14]
	3.85(7)	0.34(3)	3.57(8)	RM	[17]
21	3.99(6)	0.24(2)	3.81(6)	RS	[14]
	4.15(8)	0.31(3)	3.90(9)	RM	[17]
22	3.55(10)	0.19(3)	3.42(10)	RS	[14]
23	3.92(8)	0.23(3)	3.75(9)	RS	[14]
24	3.81(10)	0.24(3)	3.63(10)	RS	[14]
25	4.01(21)	0.22(3)	3.85(21)	RS	This work
			Dimer dissociation		
9	4.59(8)	1.06(9)	3.66(12)	BS	[18]
11	4.91(11)	0.77(8)	4.27(14)	BS	[18]
13	4.99(9)	0.62(7)	4.50(11)	BS	[18]
15	4.72(10)	0.56(6)	4.29(12)	BS	[18]

[a]The slightly larger uncertainties of the previously published dissociation energies were calculated differently than in the present work, where the statistical and systematic uncertainties are always added in square.

[b]The dissociation energy value $D_N=3.36(6)$ eV for $N=17$ cited in Ref. [17] differs by a small rounding error.

Details of the procedure are described in Refs. [14,17], and a discussion of the calculations of the relatively small kinetic energy release can be found in Refs. [17,74].

IV. DISSOCIATION ENERGIES FROM DECAY RATES

A single measured rate constant allows the extraction of the dissociation energy provided some parameters of the decaying system are known. These are the capture cross section σ_{N-1} for the inverse process

$$Au_{N-1}^+ + Au \rightarrow Au_N^+ \tag{3}$$

and the level densities of the reacting cluster and the product. In the absence of competing decay channels, the measured rate constants for monomer evaporation can then be approximated as [49,50]

$$k_N(E) \simeq \frac{8\pi g \mu \sigma_{N-1}}{h^3}(k_B T_d)^2 \frac{\rho_{N-1}(E-D_N)}{\rho_N(E)}, \tag{4}$$

where $g=2$ is the electronic degeneracy of the free gold atom, μ the reduced mass of the channel, $\rho_{N-1}(E-D_N)$, $\rho_N(E)$ the level densities of the internal degrees of freedom of the species and energies indicated, and σ_{N-1} the geometric cross section for capture of an atom, $\sigma_{N-1}=\pi r_s^2[(N-1)^{1/3}+1]^2$, with the bulk value $r_s=1.59$ Å. The temperature T_d is the microcanonical temperature of the product cluster,

$$\frac{1}{k_B T_d} = \frac{d}{dE}\ln(\rho_{N-1}(E-D_N)). \tag{5}$$

The approximate nature of expression (4) relates to the cross section, which is assumed constant here (note that this approximation should not be used when calculating kinetic energy release distributions), and to the neglect of angular momentum constraints in the calculation of the phase space of the product state.

The remaining unknown quantities, the level densities, are related to the caloric curves, $E(T)$, of the clusters in the canonical ensemble. As a reference point we will use the high temperature relation $E=(3N-6)(k_B T-\hbar\omega_D/2)$, which holds for a crystal with $3N-6$ identical frequencies ω_D (Einstein crystal). The value of the Debye temperature $T_D=\hbar\omega_D/k_B$ is 165 K for the bulk [75], and we neglect the corrections introduced by a more realistic description of the vibrational modes of the clusters, and the deviation of the average frequency from the maximum of the Debye spectrum. The Einstein spectrum has the well-known high-energy level density [76]

$$\rho_N(E) = \frac{[E+(3N-6)\hbar\omega_D/2]^{3N-7}}{(3N-7)!(\hbar\omega_D)^{3N-6}}. \tag{6}$$

Inserting this into Eq. (4) gives basically the Engelking result for the rate constant [50]:

$$k_N(E) = \frac{8\pi g \mu \sigma_{N-1}}{h^3}(k_B T_d)^2 \left(\frac{\hbar\omega_D(3N-8)}{E-D_N+(3N-9)\hbar\omega_D/2}\right)^3 \times \left(\frac{E-D_N+(3N-9)\hbar\omega_D/2}{E+(3N-6)\hbar\omega_D/2}\right)^{3N-7}, \tag{7}$$

where the approximation $(3N-7)(3N-9)\approx(3N-8)^2$ was used. The quantity cubed is essentially $\hbar\omega_D/k_B T_d$, and hence

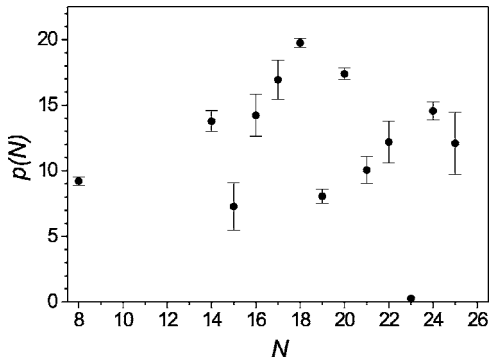

FIG. 4. The variation of the fitted dissociation energies with excitation energy, $p(N)$, as a function of cluster size N (for details see the text). Rate constants consistent with Eq. (7) require a value of zero.

$$k_N(E) = \frac{g\mu\sigma_{N-1}\omega_D^3}{\pi^2 k_B T_d}\left(\frac{E - D_N + (3N-9)\hbar\omega_D/2}{E + (3N-6)\hbar\omega_D/2}\right)^{3N-7}. \quad (8)$$

For future reference a numerical estimate is useful. With the value of σ_{N-1} and μ pertaining to the decay of $N=15$, and daughter temperatures of $k_B T_d = 0.1$ eV, the frequency factor is

$$\omega = \frac{g\mu\sigma_{N-1}\omega_D^3}{\pi^2 k_B T_d} = 3.6 \times 10^{16}\ \mathrm{s}^{-1} = e^{38.1}\ \mathrm{s}^{-1}. \quad (9)$$

Although this factor depends on size and excitation energy, the variations are relatively small for the relevant parameter values. For completeness we mention that also the electronic degeneracies in the ground state will give contributions to the value of the frequency factors. Strong odd-even effects, as those present in gold clusters, involve the spin degeneracy and the detailed balance expression in Eq. (4) gives corrections of a factor of $1/2$ for odd electron number clusters and of 2 for even electron numbers (for more details see Ref. [57]). We will disregard this effect.

The rate constant, the precise value of which obviously hinges on the physical assumptions made, was used to invert the experimental data to find the dissociation energies. In the calculations the full expression in Eq. (8) was used. A similar inversion was performed in Ref. [14] with a level density which was calculated with a slightly more complicated algorithm, yielding a presumably more precise caloric curve. The differences between the heat capacities in that calculation and the one used here are small and the quantitative conclusions are similar.

The results are twofold: First, the fitted dissociation energies show a persistent increase with the parent excitation energies [14]. A similar trend will also be reflected in the Arrhenius-type plots discussed in the following. The strength of the dependence of the dissociation energy D on the excitation energy E can be characterized by a parameter $p(N)$,

$$p(N) \equiv (3N-6)\frac{dD}{dE}. \quad (10)$$

Ideally, p should be zero, i.e., there should be no change in the resulting value of the dissociation energy when the excitation energy is varied. The factor of $3N-6$ is introduced to facilitate a comparison with the ratio of dissociation energy and temperature, i.e., the argument of the Boltzmann factor in the rate equation. This ratio is the Gspann parameter [77] discussed in the following, and takes values of typically $D/k_B T \simeq 20-30$ for experiments on the microsecond to millisecond time scale. The values of $p(N)$ are shown in Fig. 4 and are of the same order of magnitude, suggesting a strong variation of the fitted values of D with excitation energy.

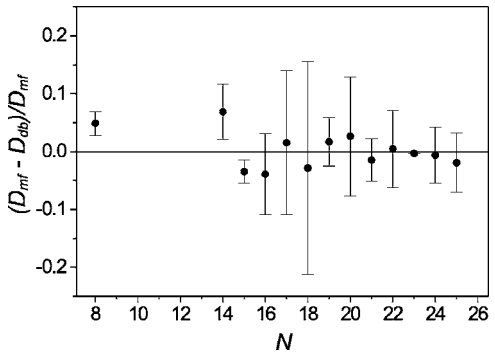

FIG. 5. Comparison of the mean dissociation energies fitted with the detailed-balance rate constant in Eq. (8) (D_{db}) and the model-free values (D_{mf}), relative to the latter. The average values close to zero indicate that the typical rate constant is well described by the detailed-balance equation with the simple harmonic level density used. The uncertainties indicate the tendency for the fitted dissociation energy to change with excitation energy.

Second, however, the absolute values of the dissociation energies deduced from the measured decay constants are close to the model-free values. To make this statement quantitative, we have calculated the mean of all fitted dissociation-energy values for all excitation energies/rate constants for the individual cluster sizes. The result is shown in Fig. 5. Given the good agreement between the average values of the dissociation energies found by inversion of the detailed balance rate constants of Eq. (8) with the model-free dissociation energies, we will apply the expression for the rate constant also to the cluster sizes for which the model-free values have not been measured.

The relevant cluster sizes are $N=7,9-13,26,27$, and the values are given in Table V. The uncertainties are estimated as twice the standard deviation of the fitted values, plus an average of 0.13 eV from the uncertainties on the model-free values for $N=8,14-25$. For the two largest clusters, $N=26,27$, where only one rate constant has been measured, the uncertainties have summarily been set to 0.4 eV.

The dissociation energy $D(N,1)$ for monomer and $D(N,2)$ for dimer evaporation are related by a thermodynamic cycle:

$$D(N,2) + D(2,1) = D(N,1) + D(N-1,1), \quad (11)$$

which allows a consistency check. For $N=9$ this gives a monomer dissociation energy of $D(9,1)=3.30(15)$ eV, where all uncertainties have been added in square. The value only depends on a single new parameter, viz. the dimer binding energy of $D(2,1)=2.29(2)$ eV [78]. The value of 3.3 eV

TABLE V. Dissociation energies calculated from the rate constants, Eq. (8), and the thermodynamic cycle, Eq. (11).

N	D_N (eV) Eq. (11)	D_N (eV) Eq. (8)
7		3.4(3)
9	3.30(15)	3.5(3)
10		2.4(2)
11	4.16(24)[a]	3.3(3)
12		2.9(3)
13	3.9(3)[a]	3.5(4)
26		3.7(4)
27		3.8(4)

[a]For the calculation the monomer dissociation energies D_N, $N=10,12$, as deduced from Eq. (8) have been used.

is in good agreement with the 3.5 eV derived from the application of Eq. (8) to the measured rate constants. For $N=11$ the values of $D(N,2)+D(2,1)$ and $D(N,1)+D(N-1,1)$ are 6.56(14) and 5.7(4) eV, and for $N=13$ they are 6.56(11) and 6.4(5) eV. The deviation for $N=11$ is twice the standard deviation, i.e., marginally significant. The remaining process for which the data can be used as a check is the decay of Au_{15}^+ for which all terms in Eq. (11) have been measured. The equality was found to hold very well [16].

Figure 6 summarizes all dissociation energies, model-free and not, and compares the values with the liquid drop approximation. The latter is calculated as

$$D_{\mathrm{LDM}}(N,1) = A - B \times [N^{2/3} - (N-1)^{2/3}] - C \times [N^{-1/3} - (N-1)^{-1/3}] \quad (12)$$

for monomer evaporation and

$$D_{\mathrm{LDM}}(N,2) = 2A - B \times [N^{2/3} - (N-2)^{2/3}] - C \times [N^{-1/3} - (N-2)^{-1/3}] - D(2,1) \quad (13)$$

for dimer evaporation where $A=3.81$ eV is the bulk cohesive energy, $B=4\pi\gamma r_s^2=3.00$ eV represents the surface energy, and $C=e^2/(8\pi\epsilon_0 r_s)=4.53$ eV is the coefficient of the classical Coulomb term [79,80].

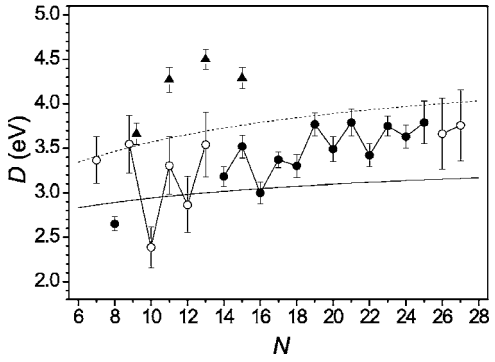

FIG. 6. Dissociation energies for Au_N^+. Closed symbols: model-free values for monomer evaporation ($N=8,14-25$, circles) and for dimer evaporation ($N=9,11,13,15$, triangles). Open circles: Averages over several excitation energies calculated with the theoretical rate constant given in Eq. (8). The bulk binding energy per atom is 3.81 eV [75] and the solid and dashed lines give the dissociation values according to the liquid drop model (LDM) as deduced with Eqs. (12) and (13), respectively.

The liquid-drop dissociation energies represent the smooth part of $D(N,1)$ reasonably well, although the difference at the high mass end is clearly significant. For the comparison, it should be kept in mind that the most important liquid drop parameters, A and B, have been determined for macroscopic bodies and the application to particles composed of a few atoms is far from guaranteed.

V. FREQUENCY FACTORS

The conclusion of the previous section is that the absolute values of the rate constants are reasonably well reproduced by the simple equations used, but that the rate constants vary too slowly with excitation energy. In terms of Arrhenius plots [14] these observations are equivalent to an approximately correct *value* of the dissociation energy $D=D(N,1)$, but an erroneous *slope* dD/dE. Thus an error in the experimental slope will give both an incorrect dissociation energy, and an incorrect extrapolation to zero inverse temperature, i.e., an incorrect frequency factor. Furthermore, these errors are correlated. Quantitatively,

$$\ln(k) = \ln(\omega) - D/k_BT \Rightarrow \ln(\omega_{\mathrm{Arrh}}) = \ln(k) + \frac{D_{\mathrm{Arrh}}}{k_BT}, \quad (14)$$

where the subscript Arrh refers to the (possibly incorrect) values derived from an Arrhenius plot. The correct value of ω corresponds to $D_{\mathrm{Arrh}}=D_{\mathrm{mf}}$, where D_{mf} are the model-free values given above. We therefore also have

$$\ln(\omega) = \ln(k) + \frac{D_{\mathrm{mf}}}{k_BT}. \quad (15)$$

Combining Eqs. (14) and (15) gives

$$\ln(\omega_{\mathrm{Arrh}}) = \ln(\omega) - \frac{D_{\mathrm{mf}} - D_{\mathrm{Arrh}}}{k_BT}. \quad (16)$$

Since, for a given cluster size, the range of temperatures covered in the experiments is reasonably small we can use a mean value, $\langle T_N \rangle$. Furthermore, we can replace this mean temperature by the ratio of the dissociation energy to the Gspann parameter G [77]:

$$k_B\langle T_N\rangle \approx D_N/G \equiv D_N/\ln(\omega\langle t\rangle), \quad (17)$$

where $\langle t\rangle$ is an average measurement time, or in this case, an average inverse rate constant. The value of D_N is the model-free dissociation energy. Hence we have

$$\ln(\omega_{\mathrm{Arrh}}) = \ln(\omega) - \ln\left(\frac{\omega}{\langle k\rangle}\right)\frac{D_{\mathrm{mf}} - D_{\mathrm{Arrh}}}{D_{\mathrm{mf}}}. \quad (18)$$

The application of the equation requires knowledge of the true dissociation energies. Conversely, if this knowledge is available it allows one to derive the value of ω, which can be obtained from a plot of $\ln(\omega_{\mathrm{Arrh}})$ vs $(D_{\mathrm{mf}}-D_{\mathrm{Arrh}})/D_{\mathrm{mf}}$. Since both the slope and the intercept depend on the frequency factor, and this is the only unknown, the plot also provides a consistency check.

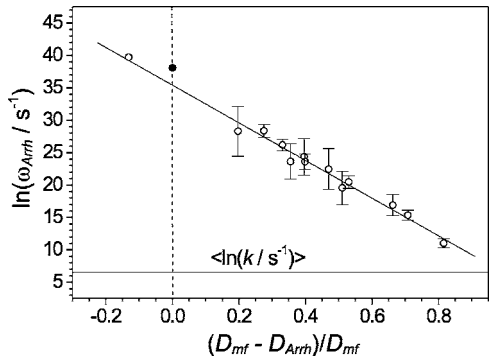

FIG. 7. The relation between the logarithm of the frequency factor and the error in fitted dissociation energy in an Arrhenius-type analysis using Eq. (20). The closed circle corresponds to the theoretically expected value of $e^{38.1}$ s^{-1}, calculated in Sec. IV. The horizontal line is the average of the logarithm of all measured rate constants. The cluster sizes are, in order of increasing abscissa, N =23,15,19,21,16,25,8,22,17,24,14,20,18.

To test the relation in Eq. (18) we have fitted the experimental rate constants as a function of the reciprocal microcanonical temperature T_m which is related to the excitation energy E as

$$(3N-7)k_B T_m = E - D_N/2 + (3N-6)\hbar\omega_D/2. \qquad (19)$$

The subtraction of $D_N/2$ is the finite heat bath correction [81]. This gives

$$k \approx \omega_{\mathrm{Arrh}} \exp[-(D_{N,Arrh} + 3\hbar\omega_D/2)/(k_B T_m)]. \qquad (20)$$

Fits of the data with this and similar equations give the large discrepancies between the model-free and fitted dissociation energies which were described in Ref. [14]. Also the values of $\ln(\omega_{\mathrm{Arrh}})$ show strong variations with cluster size. The incorrect dissociation energies here are caused by the *variation* of the experimental rate constant with energy. These values may differ strongly from dissociation energies which were extracted from the *values* of the rate constants and compared with the model-free values in Fig. 5.

As an alternative to the application of the finite heat bath correction and an Arrhenius plot, we have also analyzed the data with

$$\begin{aligned}[E + (3N-6)\hbar\omega/2] \times k_N(E)^{1/(3N-7)} \\ = \omega^{1/(3N-7)}[E + (3N-6)\hbar\omega/2] \\ - \omega^{1/(3N-7)}(D_N + 3\hbar\omega_D/2),\end{aligned} \qquad (21)$$

which is easily obtained from Eq. (8) with the abbreviation for ω used in Eq. (9). Plotting the left hand side versus $[E + (3N-6)\hbar\omega/2]$ gives straight lines with intercept and slope from which ω and D_N can be calculated.

The fits of the data with the Arrhenius expression Eq. (20) and with Eq. (21) differ somewhat, but both yield similar straight lines when Eq. (16) is plotted with the two sets of data. Figure 7 shows the data from fits with Eq. (20). Both analytical methods give intercepts for $D_{\mathrm{Arrh}} - D_{\mathrm{mf}} = 0$ of $\ln(\omega/\mathrm{s}^{-1}) = 35.4 \pm 0.5$. This value should be compared with the theoretical value in Eq. (9) calculated from the detailed-balance equation in Eq. (8), $\omega = e^{38.1}$ s^{-1}. The difference is a factor of $e^{2.7} \simeq 15$, which is a reasonably good agreement for an analysis based on Arrhenius-like plots. For comparison, an uncritical application of the fitted Arrhenius parameters gives a discrepancy of up to $e^{26} \approx 10^{11}$ [14].

The slopes of the Arrhenius fit, Eq. (20), and the fit of Eq. (21) are slightly different, -29.1 ± 1.0 and -32.3 ± 1.4, respectively, but still in reasonable agreement. After inclusion of the term $\langle \ln(k/\mathrm{s}^{-1}) \rangle = 6.5$, which is the grand total logarithmic average of the measured rate constants, the slopes give the two values $\ln(\omega/\mathrm{s}^{-1}) = 36$ and $\ln(\omega/\mathrm{s}^{-1}) = 39$, which bracket the expected value of 38.

The frequency factor derived from this analysis depends on the heat capacity used to extract the Arrhenius parameters from the measured rate constants. This dependence arises because the energy needs to be translated into a temperature. We have estimated the effect of a different heat capacity with a simple model, where all heat capacities are scaled with a factor α above the Debye temperature. This moves the points in Fig. 7 on the abscissa and changes the slope and the intercept by the same amount, $(\alpha - 1)\ln(\omega/\langle k \rangle)$. The expected frequency factor of $e^{38.1}$ s^{-1}, on the other hand, varies in the opposite direction with the amount $-3(\alpha-1)[\ln(T_d/T_D) - \alpha]$. An increase in heat capacity used in the Arrhenius fits thus increases the value fitted from the line in Fig. 7 and at the same time reduces the expected value. Given that these three values are already reasonably close, there is little room for variations of the heat capacity in this analysis of the data.

VI. COMPARISON WITH THEORETICAL BINDING ENERGIES

Before comparing our data with theoretically predicted values we should mention possible differences in the physical meaning of the experimental and theoretical values. One reason the comparison between experiments and theory could be misleading is the kinetic energy release. This is a quantity which presently is only calculated as a correction to the experimental data. If the evaporation of an atom or a dimer proceeds without any activation barrier for the reverse process, this calculation is rather robust, and possible modifications within this assumption can change the final dissociation energies only by an amount which is within the error bars. If, however, there is a reverse activation barrier for attachment this barrier will have to be added to the ground state separation energy for the process, i.e., to the difference between the ground state energies of the parent and product. The absence of a reverse barrier is consistent with the behavior of bulk gold, but that in itself does not guarantee that this is also the case for clusters. One should keep in mind that the model-free dissociation-energy values are sensitive only to the kinetic energy release in the decay of the initial cluster species in the sequential decay. The corresponding temperatures are well in excess of 1000 K and a comparison with barriers calculated at zero temperature would most likely be misleading.

The high temperature is also an important fact to keep in mind when considering isomers. This problem is particularly acute with the observation that the crossover from planar to

three-dimensional structures takes place in the calculated structures at sizes covered by our experiments, around $N=7,8$, but isomers are calculated to be present in other size clusters also [82–84]. One indication that this does not influence our values is the comparison of the dissociation energies obtained with sequential and multisequential decays. The latter has a precursor which is one atom bigger than that of the sequential decay, and consequently is excited to an energy which is higher by the corresponding dissociation energy. The dissociation energies obtained with these two variations of the method are identical within the uncertainty for all five cluster sizes for which both variations have been applied ($N=17-21$). This demonstrates that if isomers do influence the values, at least the effect is insensitive to a temperature increase of $D_N/k_B(3N-6)$ on top of already very high temperatures. The most likely explanation is that the relevant isomeric states are effectively sampled by barrier crossing.

In Ref. [85] values for monomer and dimer dissociation energies up to $N=13$ were calculated and structures selected based on a comparison with mobilities, and a comparison with our experimental data is thus possible for the sizes $N=7-13$. The picture is very clear: if the dimer dissociation energy of $N=11$ is excluded from the comparison, then six out of nine values are more than two standard deviations below the experimental values. The clusters with odd electron numbers fare worse than the even species. The theoretical result is an exaggerated odd-even structure, and a too low average value. The incorrect energies in Ref. [85] do not rule out that the associated geometric structures are correct, of course.

The data given in Ref. [86] allow the comparison only with the monomer dissociation energy of $N=8$. The value is 1.54 eV, low by 1.1 eV. This discrepancy is comparable to the one found in Ref. [85] (0.7 eV). The calculations in Ref. [87] fare quite well. The comparison encompasses monomer dissociation energies from $N=7$ to 13, and differences to the experimental values are both positive and negative. Only in the cases $N=8,9$ do the theoretical values differ from the experimental with more than 2σ, in both cases overestimating the dissociation energy.

VII. EFFECT OF RADIATIVE COOLING

At this point we have demonstrated the systematics in the failure of an Arrhenius-type analysis of the data, and have shown how this can be used to corroborate frequency factors in the rate constant equation. Furthermore, based on this systematics, we have calculated dissociation energies for species where model-free values are not available. This consistent picture was obtained with a level density which is derived from a representation of the vibrational degrees of freedom as a collection of harmonic oscillators with a known frequency.

We are still left with the task of explaining the reason for the drift of the calculated dissociation-energy values with excitation energy, as demonstrated in Fig. 4. Two possibilities present themselves. One is that the heat capacity is higher than anticipated for certain sizes. This is not a strong candidate for a correct explanation, because the data on dissociation energies in Fig. 5, based on the equipartition value of the internal heat capacity, show good average agreement with the model-free values. In addition, $\ln(k)$ versus excitation energy E has a positive curvature for most even-size (odd electron number) clusters studied with $N>12$. It is difficult, although perhaps not impossible, to reconcile this behavior with an activated process.

A second possibility is that the measured rate constant is influenced by radiative cooling [40,42,88]. We will analyze the measured rate constants with this assumption. The radiation is related to the photon-absorption cross section, σ_p, via detailed balance as [41,45,89]

$$k(E,\omega_p)d\omega_p = \frac{\omega_p^2}{\pi^2 c^2}\sigma_p(\omega_p)\frac{1}{e^{\hbar\omega_p/k_B T_{\mathrm{Rad}}}-1}d\omega_p, \qquad (22)$$

where ω_p is the photon (angular) frequency and T_{Rad} is the microcanonical temperature for radiation. For the canonical caloric curve $E=sk_BT-s\hbar\omega_D/2$, the latter is equal to $T_{\mathrm{Rad}}=(E+s\hbar\omega_D/2)/[k_B(s-1)]$, if the finite heat bath correction to photon emission is ignored. A calculation of the competing unimolecular decay and radiative cooling with all possible photon energies is a very demanding task. It may also not be unique, because the number of free parameters in the problem exceeds the number of measured points. In order to be specific, we have parametrized the photon-absorption cross section in terms of a single resonance with the semiclassical expression [89],

$$\sigma_p = \frac{fq^2}{m_e c\epsilon_0}\Gamma N_e \frac{\omega_p^2}{(\omega_p^2-\omega_s^2)^2+(\Gamma\omega_p)^2}, \qquad (23)$$

where $q=e$ is the electron charge, m_e the mass of the electron, $N_e=N-1$ the number of delocalized electrons, ω_s the position of the resonance, Γ the width of the resonance, and f the oscillator strength per electron ($0\leqslant f\leqslant 1$). The relevant part of this cross section is the low energy tail, $\omega_p^2\ll\omega_s^2$. This parametrization admittedly ignores some of the complicating and interesting features of the electronic structure of gold clusters which will influence the shape of the surface plasmon, see, e.g., Ref. [90], and references therein.

We will furthermore use the approximation that the emission of a single photon is sufficient to quench the evaporative decay. The validity of this approximation can be estimated by a calculation of the quenching effect of a photon emission. The average photon energy is $6k_BT$ [45], and the decrease in evaporative rate constant for the emission of one of these photons is therefore

$$\frac{d\ln k_{\mathrm{evap}}}{dE}(-h\nu) = -\frac{D_{\mathrm{mf}}}{C_v k_B T^2}6k_BT = -\frac{D_{\mathrm{mf}}}{C_v T}6 \simeq -\frac{60}{N-2}, \qquad (24)$$

where $C_v=k_B(3N-6)$ and $D_{\mathrm{mf}}/k_BT\simeq 30$ was used. This is numerically larger than unity for all values of N considered in this study, and we can therefore expect that the emission of a single photon does indeed quench the evaporative decay to a good approximation.

We can then write the total decay constant as the sum of the radiative and the evaporative decay constants. The cross section in Eq. (23) is to a good approximation proportional to the frequency squared, and the photoemission rate constant is consequently proportional to T^5 [89]. The total rate constant is therefore

$$k_{\mathrm{obs}} = k_{\mathrm{Rad}} + k_{\mathrm{evap}} = \beta T_{\mathrm{Rad}}^5 + k_{\mathrm{evap}}, \tag{25}$$

where

$$\beta = \frac{fq^2}{4\pi\varepsilon_0}\frac{4\times 24\zeta(5)N_e}{\pi c^3 m_e \hbar^2}\frac{\hbar\Gamma}{(\hbar\omega_s)^4} = 6.87\times 10^8 \frac{N_e f\hbar\Gamma}{(\hbar\omega_s)^4}\mathrm{s}^{-1}\ \mathrm{eV}^{-2}, \tag{26}$$

is found by integration of Eq. (22) with Eq. (23) [$\zeta(5)$ is the Riemann zeta function at $x=5$]. The value of β depends on $f\Gamma/\omega_s^4$, which will be kept as a fit parameter. The evaporative rate constant, k_{evap}, is in principle known because the dissociation energy is known and the frequency factor is fitted previously. However, the rate constant has a very strong dependence on the parameters that enter the expression, and some flexibility is required in the fitting procedure. We will use the model-free dissociation energies, and the empirical value of the frequency factor found above, and only allow the effective number of degrees of freedom as a fit parameter, i.e., we will replace $3N-7$ in Eq. (8) with the fit parameter $s-1$. From the derivation of the rate constant it is clear that this is inconsistent (the rate constant contains the ratio of level densities for two *different* clusters), but as we will see this will be a minor inconsistency. The evaporative rate constant therefore becomes

$$k_{\mathrm{evap}} = \left(\frac{E - D_N + (s-3)\hbar\omega_D/2}{E + s\hbar\omega_D/2}\right)^{s-1} e^{35.4}\ \mathrm{s}^{-1}. \tag{27}$$

The parameter s is related to the canonical heat capacity, $C_v = sk_B$, and in the harmonic limit has the value $s=3N-6$. For most cluster sizes, the fitted value agrees with this number. The typical difference is less than 10%, with the only exception being $N=18$, which exceeds the harmonic-oscillator value by 36%. This confirms that the procedure behind Eq. (25) is basically sound. The fitted heat capacities depend on the frequency factor used in the fits. Both are reasonable, however, and we will therefore accept the values of β from the fits of Eq. (25) as a reasonable estimate of the magnitude of the radiative cooling.

The fitted values of β can be solved for the ratio $f\hbar\Gamma/(\hbar\omega_s)^4$ by Eq. (26). The values vary much with size. Everything considered, we do not expect the scatter to reflect the intrinsic properties of the individual clusters, and will draw conclusions only from average values. In order to compare the model with experimental values on the photoabsorption spectra [81,89–92] of gold clusters, we have used the value $\hbar\Gamma=0.2$ eV for all N and extracted $f^{-1/4}\hbar\omega_s$. The values range from $\hbar\omega_s = 3.2f^{1/4}$ eV for $N=8$ to $9.2f^{1/4}$ eV for $N=19$, with an average of $5.7f^{1/4}$ eV.

The average expected photon energy of approximately $6k_BT$ is typically around 1 eV. This is beyond the wavelength range probed in photoabsorption experiments, and we are therefore forced to compare extrapolated absorption cross sections. In Refs. [93,94] the absorption spectra of large, deposited gold particles (diameters of 4 nm, $\geqslant$20 nm) were found to have an absorption peak at 2–2.5 eV, increasing with decreasing radius. No oscillator strengths were reported, but the width of the resonance was measured as a function of size in Ref. [94], and show a decreasing trend with decreasing size, reaching a value of approximately 0.3 eV ($=2\hbar\Gamma$) in the 20–40 nm region. A blueshift was already seen in the early measurements reported in Ref. [92], where depletion spectroscopy was used to measure the absorption profile of neutral and positively charged Au_N, $N=7,9,11,13$. These data (for $N\geqslant 9$) show an absorption peak around 3×10^4 cm^{-1}=3.7 eV, and a width of approximately 1 eV. This peak resides on top of the low-energy side of a partly measured strong absorption in the UV. For the odd-electron number neutral clusters (still with $N\geqslant 9$), the spectra are virtually identical apart from the appearance of a smaller peak around 2.7 eV. Consistent with the presence of a large blue component, the measured oscillator strength falls short of 100%. For odd electron numbers, f is approximately 0.025, and for even electron numbers it is 0.01. Hence $f^{1/4}$ is between 0.3 and 0.4 for both parities, and by use of a common value of 0.35 for both, with the average fitted value of $\hbar\omega_s = f^{1/4}5.7$ eV, this gives a value $\hbar\omega_s \simeq 2.0$ eV.

This value is below the resonance energies of 3.7 and 2.7 eV measured in Ref. [92] for the even and odd electron number clusters, respectively, suggesting that the radiative cooling is higher than measured in these experiments. One possible explanation for this is that in the experiments in Ref. [92], the temperatures of the clusters are low compared with the temperatures relevant for our data. Elevated temperatures are expected to smear absorption profiles locally, giving a stronger tail to the low energy side, effectively reducing the resonance energy fitted from our data. This effect is presumably also at work for the large UV component which appears to carry considerable oscillator strength. A quantitative estimate of this effect is beyond the scope of this article.

VIII. CONCLUSIONS

Rate constants and monomer-dimer branching ratios for decays of positively charged gold clusters have been presented, from which a range of model-free dissociation energies have been determined previously. Several new values have been derived, based on the observed behavior of the measured rate constants and a detailed balance rate constant. Frequency factors and dissociation energies have been extracted from two different Arrhenius-type schemes, with a persistent and serious discrepancy between expected and observed fit parameters. The errors in the Arrhenius-based dissociation energies were found to correlate strongly with the value of the fitted frequency factor. This correlation was used to extract an experimental value for the frequency factor which is in good agreement with the value expected from detailed balance. The failure of the Arrhenius analysis was suggested to be due to the presence of radiative cooling. The data were fitted with this assumption and a simplified model with a single resonance frequency. This frequency was found to be lower than observed in low temperature spectroscopic studies, but of the right order of magnitude.

ACKNOWLEDGMENTS

This work was funded by VR, the Deutsche Forschungsgemeinschaft (Collaborative Research Center SFB652), and the EU network "CLUSTER COOLING" (HPRN-CT-2000-0026). Comments on the manuscript by O. Echt are gratefully acknowledged.

[1] I. Katakuse, T. Ichihara, Y. Fujita, T. Matsuo, T. Sakurai, and H. Matsuda, Int. J. Mass Spectrom. Ion Process. **67**, 229 (1985).
[2] M. D. Morse, Chem. Rev. (Washington, D.C.) **86**, 1049 (1986).
[3] K. Fauth, U. Kreibig, and G. Schmidt, Z. Phys. D **12**, 515 (1989).
[4] H. Feld, A. Leute, D. Rading, A. Benninghoven, and G. Schmid, Z. Phys. D: At., Mol. Clusters **17**, 73 (1990).
[5] A. Selinger, P. Schnabel, W. Wiese, and M. P. Irion, Ber. Bunsenges. Phys. Chem. **94**, 1278 (1990).
[6] J. Ho, K. M. Ervin, and W. C. Lineberger, J. Chem. Phys. **93**, 6987 (1990).
[7] I. Rabin, C. Jackschath, and W. Schulze, Z. Phys. D **19**, 153 (1991).
[8] C. Jackschath, I. Rabin, and W. Schulze, Ber. Bunsenges. Phys. Chem. **96**, 1200 (1992).
[9] K. J. Taylor, C. L. Pettiette-Hall, O. Cheshnovsky, and R. E. Smalley, J. Chem. Phys. **96**, 3319 (1992).
[10] M. Hermann, U. Kreibig, and G. Schmidt, Z. Phys. D **26**, 1 (1993).
[11] H. S. Kim, T. D. Wood, A. G. Marshall, and J. Y. Lee, Chem. Phys. Lett. **224**, 589 (1994).
[12] C. L. Cleveland, U. Landman, M. N. Shafigullin, P. W. Stephens, and R. L. Whetten, Z. Phys. D **40**, 503 (1997).
[13] M. Haruta, Catal. Today **36**, 153 (1997).
[14] M. Vogel, K. Hansen, A. Herlert, and L. Schweikhard, Phys. Rev. Lett. **87**, 013401 (2001).
[15] M. Vogel, K. Hansen, A. Herlert, and L. Schweikhard, Chem. Phys. Lett. **346**, 117 (2001).
[16] M. Vogel, K. Hansen, A. Herlert, and L. Schweikhard, J. Phys. B **36**, 1073 (2003).
[17] M. Vogel, K. Hansen, A. Herlert, and L. Schweikhard, Phys. Rev. A **66**, 033201 (2002).
[18] M. Vogel, K. Hansen, A. Herlert, and L. Schweikhard, Eur. Phys. J. D **21**, 163 (2002).
[19] M. Vogel, K. Hansen, A. Herlert, L. Schweikhard, and C. Walther, J. Chem. Phys. **116**, 9658 (2002).
[20] P. Schwerdtfeger, J. S. McFeaters, M. J. Liddell, J. Hrusak, and H. Schwarz, J. Chem. Phys. **103**, 245 (1995).
[21] O. D. Häberlen, S. C. Chung, M. Stener, and N. Rösch, J. Chem. Phys. **106**, 5189 (1997).
[22] I. L. Garzón, K. Michaelian, M. R. Beltrán, A. Posada-Amarillas, P. Ordejón, E. Artacho, D. Sánchez-Portal, and J. M. Soler, Phys. Rev. Lett. **81**, 1600 (1998).
[23] H. Häkkinen and U. Landman, Phys. Rev. B **62**, R2287 (2000).
[24] N. T. Wilson and R. L. Johnston, Eur. Phys. J. D **12**, 161 (2000).
[25] H. Grönbeck and W. Andreoni, J. Chem. Phys. **262**, 1 (2000).
[26] J. R. Brown, P. Schwerdtfeger, D. Schröder, and H. Schwarz, J. Am. Soc. Mass Spectrom. **13**, 485 (2002).
[27] H. Häkkinen, B. Yoon, U. Landman, X. Li, H. J. Zhai, and L. S. Wang, J. Phys. Chem. A **107**, 6168 (2003).
[28] M. Johansson, D. Sundholm, and J. Vaara, Angew. Chem., Int. Ed. **43**, 2678 (2004).
[29] H. P. Mao, H. Y. Wang, Ni-Yu, G. L. Xu, M. Z. Ma, Z. H. Zhu, and Y. J. Tang, Acta Phys. Sin. **53**, 1766 (2004).
[30] J. Rogan, R. Ramírez, A. H. Romero, and M. Kiwi, Eur. Phys. J. D **28**, 219 (2004).
[31] H. Häkkinen, M. Moseler, O. Kostko, N. Morgner, M. A. Hoffmann, and B. Issendorff, Phys. Rev. Lett. **93**, 093401 (2004).
[32] A. V. Walker, J. Chem. Phys. **122**, 094310 (2005).
[33] P. Koskinen, H. Häkkinen, G. Seifert, S. Sanna, T. Frauenheim, and M. Moseler, New J. Phys. **8** (2006).
[34] W. Ekardt, Phys. Rev. Lett. **52**, 1925 (1984).
[35] S. Wei, W. B. Tzeng, and A. W. Castleman, J. Chem. Phys. **92**, 332 (1990).
[36] B. Concina, K. Gluch, S. Matt-Leubner, O. Echt, P. Scheier, and T. D. Märk, Chem. Phys. Lett. **407**, 464 (2005).
[37] F. Chandezon, P. M. Hansen, C. Ristori, J. Pedersen, J. Westergaard, and S. Bjørnholm, Chem. Phys. Lett. **277**, 450 (1997).
[38] K. Hansen and U. Näher, Phys. Rev. A **60**, 1240 (1999).
[39] L. Schweikhard, K. Hansen, A. Herlert, M. D. Herráiz Lablanca, and M. Vogel, Eur. Phys. J. D **36**, 179 (2005).
[40] U. Frenzel, A. Roggenkamp, and D. Kreisle, Chem. Phys. Lett. **240**, 109 (1995).
[41] K. Hansen and E. E. B. Campbell, Phys. Rev. E **58**, 5477 (1998).
[42] C. Walther, G. Dietrich, W. Dostal, K. Hansen, S. Krückeberg, K. Lützenkirchen, and L. Schweikhard, Phys. Rev. Lett. **83**, 3816 (1999).
[43] B. M. Smirnov and H. Weidele, JETP **89**, 1030 (1999).
[44] J. U. Andersen, E. Bonderup, K. Hansen, P. Hvelplund, B. Liu, U. V. Pedersen, and S. Tomita, Eur. Phys. J. D **24**, 191 (1999).
[45] J. U. Andersen, E. Bonderup, and K. Hansen, J. Phys. B **35**, R1 (2002).
[46] M. Schmidt, R. Kusche, W. Kronmüller, B. von Issendorff, and H. Haberland, Phys. Rev. Lett. **79**, 99 (1997).
[47] G. A. Breaux, C. M. Neal, B. Cao, and M. F. Jarrold, Phys. Rev. Lett. **94**, 173401 (2005).
[48] K. Hansen, A. Herlert, L. Schweikhard, and M. Vogel, Int. J. Mass. Spectrom. **227**, 87 (2003).
[49] V. Weisskopf, Phys. Rev. **52**, 259 (1937).
[50] P. C. Engelking, J. Chem. Phys. **87**, 936 (1987).
[51] K. Hansen, Philos. Mag. B **79**, 1413 (1999).
[52] R. A. Marcus, J. Chem. Phys. **20**, 359 (1952).
[53] C. E. Klots, J. Phys. Chem. **75**, 1526 (1971).
[54] W. Forst, *Unimolecular Reactions: A Concise Introduction* (Cambridge University Press, Cambridge, 2003).

[55] S. Bjørnholm, J. Borggreen, O. Echt, K. Hansen, J. Pedersen, and H. D. Rasmussen, Z. Phys. D **19**, 47 (1991).
[56] O. Genzken and M. Brack, Phys. Rev. Lett. **67**, 3286 (1991).
[57] K. Hansen and M. Manninen, J. Chem. Phys. **101**, 10481 (1994).
[58] A. A. Shvartsburg, J. H. Frederick, and K. M. Ervin, J. Chem. Phys. **104**, 8470 (1996).
[59] A. Rytkönen and M. Manninen, J. Chem. Phys. **113**, 4647 (2000).
[60] H. Weidele, U. Frenzel, T. Leisner, and D. Kreisle, Z. Phys. D **20**, 411 (1991).
[61] G. Savard, S. Becker, G. Bollen, H. J. Kluge, R. B. Moore, Th. Otto, L. Schweikhard, H. Stolzenberg, and U. Wiess, Phys. Lett. A **158**, 247 (1991).
[62] L. Schweikhard, K. Hansen, A. Herlert, M. D. Herráiz Lablanca, G. Marx, and M. Vogel, Int. J. Mass. Spectrom. **219**, 363 (2002).
[63] L. Schweikhard *et al.*, Phys. Scr., T **59**, 236 (1995).
[64] L. Schweikhard, S. Krückeberg, K. Lützenkirchen, and C. Walther, Eur. Phys. J. D **9**, 15 (1999).
[65] St. Becker, K. Dasgupta, G. Dietrich, H. J. Kluge, S. Kuznetsov, M. Lindinger, K. Lützenkirchen, L. Schweikhard, and J. Ziegler, Rev. Sci. Instrum. **66**, 4902 (1995).
[66] S. Krückeberg, G. Dietrich, K. Lützenkirchen, L. Schweikhard, C. Walther, and J. Ziegler, Int. J. Mass Spectrom. Ion Process. **155**, 141 (1996).
[67] O. Ingolfsson, U. Busolt, and K. Sugawara, J. Chem. Phys. **112**, 4613 (2000).
[68] V. A. Spasov, Y. Shi, and K. M. Ervin, Chem. Phys. **262**, 75 (2000).
[69] S. Krückeberg, L. Schweikhard, G. Dietrich, K. Lützenkirchen, C. Walther, and J. Ziegler, J. Chem. Phys. **114**, 2955 (2001).
[70] M. Vogel, A. Herlert, and L. Schweikhard, J. Am. Soc. Mass Spectrom. **14**, 614 (2003).
[71] M. Vogel, K. Hansen, A. Herlert, and L. Schweikhard, Eur. Phys. J. D **16**, 73 (2001).
[72] M. Vogel, K. Hansen, A. Herlert, and L. Schweikhard, Appl. Phys. B: Lasers Opt. **73**, 411 (2001).
[73] U. Hild, G. Dietrich, S. Krückeberg, M. Lindinger, K. Lützenkirchen, L. Schweikhard, C. Walther, and J. Ziegler, Phys. Rev. A **57**, 2786 (1998).
[74] K. Hansen, Chem. Phys. Lett. **383**, 270 (2004).
[75] C. Kittel, *Introduction to Solid State Physics*, 7th ed. (Wiley, New York, 1996).
[76] P. C. Haarhoff, Mol. Phys. **7**, 101 (1963).
[77] K. Hansen and E. E. B. Campbell, Int. J. Mass. Spectrom. **233**, 215 (2004).
[78] G. A. Bishea and M. D. Morse, J. Chem. Phys. **95**, 5646 (1991).
[79] J. P. Perdew, Phys. Rev. B **37**, 6175 (1988).
[80] M. Brack, Rev. Mod. Phys. **65**, 677 (1993).
[81] C. E. Klots, Int. Rev. Phys. Chem. **15**, 205 (1996).
[82] R. Rousseau, G. Dietrich, S. Krückeberg, K. Lützenkirchen, D. Marx, L. Schweikhard, and C. Walther, Chem. Phys. Lett. **295**, 41 (1998).
[83] G. Dietrich, S. Krückeberg, K. Lützenkirchen, L. Schweikhard, and C. Walther, J. Chem. Phys. **112**, 752 (2000).
[84] R. Rousseau and D. Marx, J. Chem. Phys. **112**, 761 (2000).
[85] S. Gilb, P. Weis, F. Furche, R. Ahlrichs, and M. M. Kappes, J. Chem. Phys. **116**, 4096 (2001).
[86] F. Remacle and E. S. Kryachko, J. Chem. Phys. **122**, 044304 (2005).
[87] E. M. Fernandez, J. M. Soler, I. L. Garzon, and L. C. Balbas, Phys. Rev. B **70**, 165403 (2004).
[88] K. Hansen, A. Herlert, L. Schweikhard, M. Vogel, and C. Walther, Eur. Phys. J. D **34**, 67 (2005).
[89] J. U. Andersen and E. Bonderup, Eur. Phys. J. D **11**, 413 (2000).
[90] V. Kasperovich and V. V. Kresin, Philos. Mag. B **78**, 385 (1998).
[91] M. Lindinger, K. Dasgupta, G. Dietrich, S. Krückeberg, S. Kuznetsov, K. Lützenkirchen, L. Schweikhard, C. Walther, and J. Ziegler, Z. Phys. D **40**, 347 (1997).
[92] B. A. Collings, K. Athanassenas, D. Lacombe, D. M. Rayner, and P. A. Hackett, J. Chem. Phys. **101**, 3506 (1994).
[93] R. Antoine, M. Pellarin, B. Palpant, M. Broyer, B. Prevel, P. Galletto, P. F. Brevet, and H. H. Girault, J. Appl. Phys. **84**, 4532 (1998).
[94] C. Sönnichsen, T. Franzl, T. Wilk, G. von Plessen, and J. Feldmann, New J. Phys. **4**, 93 (2002).